

See discussions, stats, and author profiles for this publication at: <https://www.researchgate.net/publication/235739022>

Quinoline Driven Fluorescence Turn On 1,3-Bis-calix[4]arene Conjugate-Based Receptor to Discriminate Fe³⁺ from Fe²⁺

ARTICLE in ANALYTICAL CHEMISTRY · FEBRUARY 2013

Impact Factor: 5.64 · DOI: 10.1021/ac400059w · Source: PubMed

CITATIONS

16

READS

113

6 AUTHORS, INCLUDING:



Rakesh Pathak

University of Georgia

25 PUBLICATIONS 342 CITATIONS

[SEE PROFILE](#)



Atul Gajanan Thawari

Indian Institute of Technology Bombay

3 PUBLICATIONS 17 CITATIONS

[SEE PROFILE](#)



Santanu Kumar Basu

Universität des Saarlandes

7 PUBLICATIONS 73 CITATIONS

[SEE PROFILE](#)

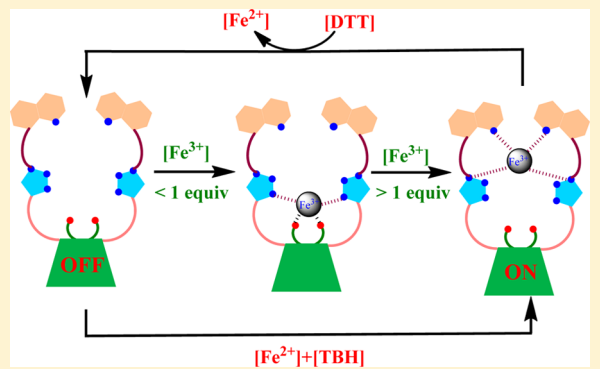
Quinoline Driven Fluorescence Turn On 1,3-Bis-calix[4]arene Conjugate-Based Receptor to Discriminate Fe^{3+} from Fe^{2+}

Rakesh Kumar Pathak,[†] Jayaraman Dessimou,[†] Vijaya Kumar Hinge,[‡] Atul Gajanan Thawari,[†] Santanu Kumar Basu,[§] and Chebrolu Pulla Rao^{*,†,‡}

[†]Department of Chemistry, [‡]Department of Biosciences & Bioengineering, and [§]Department of Chemical Engineering, Indian Institute of Technology Bombay, Powai, Mumbai 400076, India

Supporting Information

ABSTRACT: The synthesis and characterization of a triazole linked quinoline appended calix[4]arene conjugate, L, and its fluorescence turn on receptor property for Fe^{3+} have been demonstrated. The selective and sensitive discrimination of Fe^{3+} has been shown using fluorescence and absorption titration experiments. The Fe^{3+} binding to L has been further shown by ITC and ESI MS. The mode of binding of Fe^{3+} by calix[4]arene conjugate has been shown by absorption, ¹H NMR and visual color change and the species were modeled based on DFT computations. The {L + Fe³⁺} has been shown to label cells with fluorescence imaging. Moreover the utility of this conjugate has been demonstrated by the combination logic gate system.



Iron is one of the most widely distributed and crucial elements of human life.¹ In biological systems, it plays a vital role by being present as a cofactor in various proteins, owing to its easy redox reaction between Fe^{2+} and Fe^{3+} . Iron is involved in the stimulation of reactive oxygen species, which induces the lipid peroxidation, mitochondrial dysfunction, and DNA fragmentation to degrade the cellular contents and thereby causes cell death.² Thus, the discrimination between +2 and +3 is important in order to understand the biological functions regulated by iron. Imbalance in the homeostasis of this can cause various diseases and severe infections and thus can also be used for the diagnosis of a particular disease related to iron. Thus, the detection and discrimination of Fe^{3+} from other ions including Fe^{2+} at lower concentration has potential applications in the environment as well as in biological systems in order to decipher several correlated events.³ A number of molecular receptors reported in the literature suffer from one or more of the following three major aspects, viz., quenching of fluorescence, interference by other metal ions such as Cu^{2+} , and higher concentration being the detection limit.⁴ The rhodamine-based systems sense Fe^{3+} by ring cleavage and not by binding.⁵ Therefore, the development of an organic molecular system that can selectively recognize Fe^{3+} through exhibiting fluorescence enhancement is challenging to synthetic chemists and to molecular recognition scientists. Herein, for the first time, we report a quinoline-appended triazole linked calix[4]arene conjugate (L) as a fluorescence turn on as well as a visually detectable receptor for Fe^{3+} among the different metal ions studied, including Fe^{2+} . The role of the quinoline moiety has been delineated by a comparison of the results obtained from a control molecular system that possesses a pyridyl moiety

in place of the quinoline moiety. On the other hand, the role of the calix[4]arene platform has been addressed by making a noncalix[4]arene-based analog of this. The present system has also been developed to exhibit molecular logic gate properties.

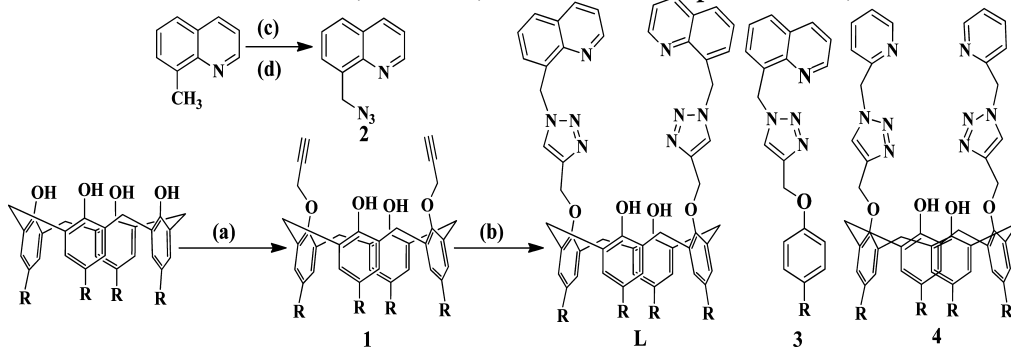
Materials and Methods. ¹H and ¹³C NMR spectra were measured on a Varian Mercury NMR spectrometer working at 400 MHz. The mass spectra were recorded on a Q-TOF micromass (YA-105), using an electrospray ionization method. Steady-state fluorescence spectra were measured on a Perkin-Elmer LS55 spectrofluorimeter. The absorption spectra were measured on a Varian Cary 100 Bio instrument. All the solvents used were of HPLC grade and were dried by routine procedures immediately before use. All the metal salts, viz. $\text{NaClO}_4 \cdot \text{H}_2\text{O}$, KClO_4 , $\text{Ca}(\text{ClO}_4)_2 \cdot 4\text{H}_2\text{O}$, $\text{Mg}(\text{ClO}_4)_2 \cdot 6\text{H}_2\text{O}$, $\text{Mn}(\text{ClO}_4)_2 \cdot 6\text{H}_2\text{O}$, $\text{Fe}(\text{ClO}_4)_2 \cdot x\text{H}_2\text{O}$, $\text{Fe}(\text{ClO}_4)_3 \cdot x\text{H}_2\text{O}$, $\text{Co}(\text{ClO}_4)_2 \cdot 6\text{H}_2\text{O}$, $\text{Ni}(\text{ClO}_4)_2 \cdot 6\text{H}_2\text{O}$, $\text{Cu}(\text{ClO}_4)_2 \cdot 6\text{H}_2\text{O}$, $\text{Hg}(\text{ClO}_4)_2 \cdot 4\text{H}_2\text{O}$, $\text{Zn}(\text{ClO}_4)_2 \cdot 6\text{H}_2\text{O}$, $\text{Cd}(\text{ClO}_4)_2 \cdot \text{H}_2\text{O}$, $\text{Cr}(\text{OAc})_3$, $\text{Al}_2(\text{SO}_4)_3 \cdot 18\text{H}_2\text{O}$, *tert*-butyl hydroperoxide (TBH), and dithiothreitol (DTT), were purchased from Sigma Chem. Company. All the fluorescence titrations were carried out in a 1 cm quartz cell by using 30 μL of calix[4]arene conjugate (L) (10^{-4} M), and the total volume in each measurement was made to 3 mL to give a final concentration of the ligand as 1 μM . During the titration, the concentration of the metal ion has been varied accordingly to result in requisite mole ratios of metal ion to L, and the total volume of the solution was maintained at 3 mL in each case by the addition of acetonitrile.

Received: January 8, 2013

Accepted: February 26, 2013

Published: February 26, 2013



Scheme 1. Synthesis of the Precursor Molecules, Reference, and the Final Receptor Molecule, L^a

^aSynthesis of receptor L: (a) propargyl bromide, K₂CO₃, acetone, reflux, 24 h, 82%; (b) 8-(azidomethyl)quinoline (3), CuSO₄·5H₂O, and sodium ascorbate in *t*-BuOH and water, rt, 12 h. R = *tert*-butyl (1:1), rt, 12 h; (c) N-bromosuccinimide, CCl₄, 5 h, reflux; (d) NaN₃, DMF, rt, 12 h, R = *tert*-butyl.

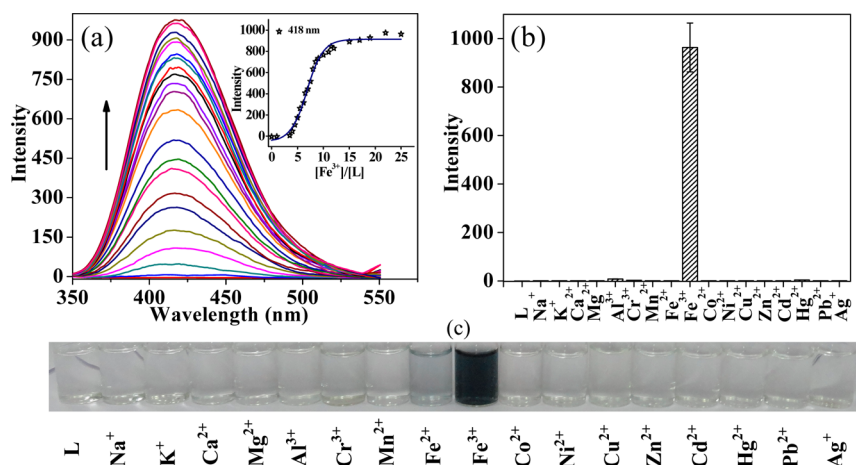


Figure 1. (a) Fluorescence spectra obtained during the titration of L with Fe³⁺ in acetonitrile, $\lambda_{\text{ex}} = 310$ nm, [L] = 1 μM . The inset shows the relative fluorescence intensity (I/I_0) as a function of the $[\text{Fe}^{3+}]/[\text{L}]$ mole ratio. (b) Histogram showing the relative fluorescence response of L in the presence of different metal ions, [L] = 1 μM ; $[\text{M}^{2+}] = 10 \mu\text{M}$. (c) The visual color change of L in the presence of different metal ions at a 1:1 stoichiometry ratio under daylight, [L] = 0.75 mM.

For absorption studies, the final concentration of [L] was kept constant at 5 μM , and all the other titration details are the same as that used for fluorescence titrations. The in situ prepared iron(III)complex of L (L: Fe³⁺ = 1:10) has been used for the titration of [FeL] with DTT. The mixture of [Fe²⁺ + L] was used for the titration with *tert*-butyl hydroperoxide (TBH) for oxidation experiments.

The calorimetric titrations were performed at 25 °C with a microcal iTC₂₀₀ isothermal titration calorimeter procured from MicroCal (Northampton, MA, USA) by taking 1 mM Fe³⁺ solution in a syringe and 0.075 mM L in the calorimeter cell. Successive additions of 2 μL of Fe³⁺ were given with a duration of 4 s and spacing of 250 s interval to allow the exothermic/ endothermic peak resulting from the interaction to return to the baseline. The ITC data were fitted with Origin provided by MicroCal by using one set of sites curve fitting models. Each time, a control is carried out without taking L, and this is subtracted from the main titration data; the resultant data is subjected to the curve fitting. The experiment has been repeated three times and average values have been reported.

The materials required for the cell culture work, viz. Dulbecco's Modified Eagle's Medium (DMEM) [catalog no. AL007A], fetal bovine serum (FBS) [catalog no. RM1112], DPBS (Dulbecco's phosphate buffered saline) without calcium

and magnesium [catalog no. TL1006], trypsin-EDTA [catalog no. TCL007], penicillin-streptomycin [catalog no. A001A], and paraformaldehyde [catalog no. RM3660], were obtained from HiMedia Laboratories, Mumbai, India. MDA-MB-231 cells were obtained from the National Centre for Cell Science, Pune, India and were cultured in the complete medium at 37 °C under a 5% CO₂ atmosphere. The complete medium comprised of DMEM supplemented with 10% FBS, 1% antibiotics.

Synthesis and characterization of L. Calix[4]arene-based dipropargyl ether (1, 2.19 g, 3.02 mmol) was added to a solution of 8-azidomethyl quinoline (2, 1.17 g, 6.36 mmol) in 100 mL of *t*-BuOH and water (1:1) mixture. To this solution, CuSO₄·5H₂O (90.48 mg, 0.36 mmol) and sodium ascorbate (0.239 g, 1.20 mmol) were added. The resulting solution was stirred for 12 h at room temperature. Upon completion of the reaction (as judged based on TLC), the organic layer was separated and the aqueous layer was extracted with dichloromethane (2 × 50 mL). The combined organic layer was washed with saturated aqueous EDTA solution, brine (2 × 100 mL), dried over anhydrous Na₂SO₄, and the solvent was removed in vacuo. The crude product was purified by column chromatography using petroleum ether and ethyl acetate followed by recrystallization from a chloroform:methanol (3:1) mixture,

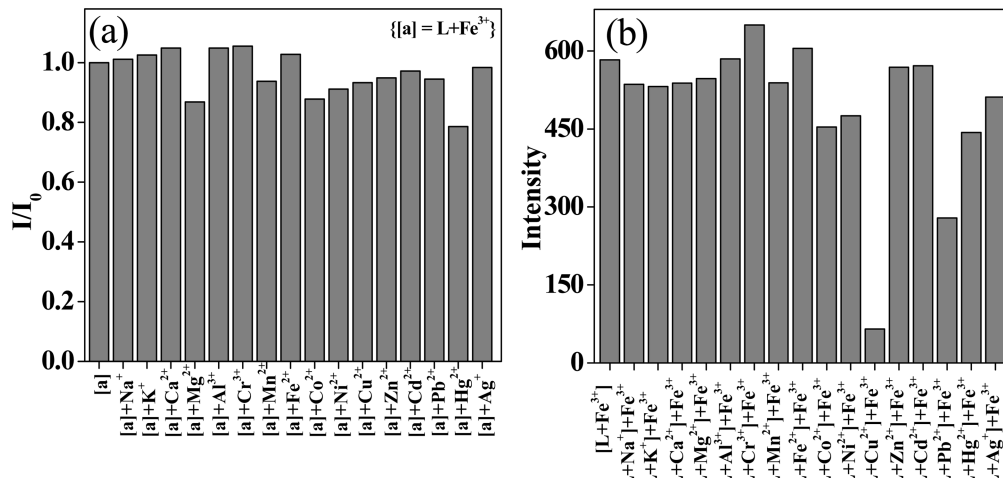


Figure 2. Histogram showing the competitive fluorescence titration responses of **L** with Fe^{3+} in the presence of various metal ions. (a) $\{\text{[L} + \text{Fe}^{3+}\} + \text{M}^{n+}\}$; $[\text{L}] = 1 \mu\text{M}$, $[\text{Fe}^{3+}] = 10 \mu\text{M}$; $[\text{M}^{n+}] = 30 \mu\text{M}$. (b) $\{\text{[L} + \text{M}^{n+}\} + \text{Fe}^{3+}\}$; $[\text{L}] = 1 \mu\text{M}$, $[\text{Fe}^{3+}] = 10 \mu\text{M}$; $[\text{M}^{n+}] = 30 \mu\text{M}$.

giving rise to a colorless solid product. Yield: 2.50 g (76%). ^1H NMR (CDCl_3 , 400 MHz): 8.82 (dd, 2H, Quin-H), 8.07 (s, 2H, triazole-H), 8.05 (d, 2H, Quin-H), 7.76 (dd, 2H, Quin-H), 7.58 (dd, 2H, Quin-H), 7.45 (m, 2H, Quin-H), 7.31 (m, 2H, Quin-H), 6.93 (s, 4H, Ar-H), 6.90 (Ar-OH), 6.66 (s, 4H, Ar-H), 6.16 (Ar-O-CH₂), 5.10 (s, 4H, AMQ-CH₂), 4.03 (d, 4H, Ar-CH₂-Ar), 3.06 (d, 4H, Ar-CH₂-Ar), 1.28 [s, 18H, Ar-C(CH₃)₃], 0.900 [s, 18H, Ar-C(CH₃)₃]. ^{13}C NMR (CDCl_3 , 100 MHz) δ (ppm): 31.0, 31.8, 31.9, 33.9, 50.2, 69.9, 121.6, 124.5, 125.1, 125.6, 126.4, 127.8, 128.3, 128.9, 128.9, 129.8, 132.5, 133.4, 136.2, 141.5, 144.0, 145.8, 147.1, 149.7, 150.3, 150.5; m/z (ES/MS) 1116.7 ([M + Na]⁺ 100%). HRMS (EI): m/z calcd for $\text{C}_{70}\text{H}_{77}\text{N}_8\text{O}_4$: [M + H], 1093.6068; found, 1093.6066.

RESULTS AND DISCUSSION

The main receptor molecule, **L**, was synthesized as given in Scheme 1, and the control molecules, viz. **3** and **4**, were synthesized in an analogous manner (Figure S01 of the Supporting Information). All these conjugates were characterized by various spectral and analytical techniques, such as ^1H and ^{13}C NMR and HRMS (Figures S02–S04 of the Supporting Information). The calix[4]arene-based derivatives were found to be in the cone conformation as observed from the NMR spectral data.

To understand the ion receptor properties of **L**, studies were carried out by emission, absorption, and ^1H NMR spectroscopy, and the species of recognition has been addressed by mass spectrometry and computations based on the density functional theory (DFT). Fluorescence spectroscopy was used for evaluating the receptor ability of **L** toward metal ions, such as Na^+ , K^+ , Ca^{2+} , Mg^{2+} , Al^{3+} , Cr^{3+} , Mn^{2+} , Fe^{2+} , Fe^{3+} , Co^{2+} , Ni^{2+} , Cu^{2+} , Zn^{2+} , Cd^{2+} , Hg^{2+} , Pb^{2+} , and Ag^+ , at a 1 μM cuvette concentration, by exciting the solutions at 310 nm in acetonitrile followed by measuring the emission from 330 to 550 nm. Upon the addition of Fe^{3+} to **L**, the fluorescence intensity starts increasing at 418 nm and the same approaches to about 800–900 fold at saturation. No other metal ion present in this list induces any fluorescence increase in **L** (Figure 1 and Figure S05 of the Supporting Information). A thousand-fold increase observed in the quantum yield (QY) of $\{\text{L} + \text{Fe}^{3+}\}$ (0.119 ± 0.02) as compared to that of **L** ($1.3 \times$

10^{-4}) supports the fluorescence enhancement of **L** observed in the presence of Fe^{3+} , suggesting a sensitive and selective recognition of Fe^{3+} by **L** when compared to all other metal ions studied. Even the trivalent ions, such as Al^{3+} and Cr^{3+} , showed no fluorescence enhancement during the titration with **L**. On the basis of the Benesi–Hildebrand equation,⁶ the association constant for the binding of **L** by Fe^{3+} was established with $K_a = (2.2 \pm 0.1) \times 10^5 \text{ M}^{-1}$. The sensitivity of **L** for Fe^{3+} has been further evaluated by measuring the lowest concentration, using the linear dynamic response. The detection limit (LOD) and quantification limit (LOQ) were measured to be $0.334 \pm 0.020 \mu\text{M}$ ($3\sigma/\text{slope}$) and $1.135 \pm 0.045 \mu\text{M}$ ($10\sigma/\text{slope}$), respectively, suggesting its applicability to detect Fe^{3+} , even in the lower micromolar range. To our knowledge, this is the first calix[4]arene conjugate that brings fluorescence enhancement with high sensitivity toward Fe^{3+} (Figure S06 of the Supporting Information). The reason for the sensitivity has been attributed to its selective binding as addressed through absorption, MS, NMR, and computational studies. The colorless solution of **L** turns to dark blue only in presence of Fe^{3+} and not any other metal ion from the list of these seventeen ions (Figure 1). Therefore, Fe^{3+} can easily be differentiated by the naked eye from the other metal ions in the presence of **L**.

Competitive Metal Ion Titrations. In order to show the practical utility of **L** to detect Fe^{3+} selectively, even in the presence of other metal ions including Fe^{2+} , competitive metal ion titrations were carried out in two different ways. In one, the $[\text{L} + \text{Fe}^{3+}]$ was titrated with different M^{n+} ($\text{M} = \text{Na}^+$, K^+ , Ca^{2+} , Mg^{2+} , Al^{3+} , Cr^{3+} , Mn^{2+} , Fe^{2+} , Co^{2+} , Ni^{2+} , Cu^{2+} , Zn^{2+} , Cd^{2+} , Hg^{2+} , Pb^{2+} , and Ag^+), and in the other, the $[\text{L} + \text{M}^{n+}]$ mixture was titrated with Fe^{3+} . In the first, the fluorescence intensity of $[\text{L} + \text{Fe}^{3+}]$ mixture was unaltered in presence of other metal ions. In the second, the fluorescence intensity of $[\text{L} + \text{M}^{n+}]$ has been increased as a function of the addition of Fe^{3+} , except in the case of Cu^{2+} and to some extent in the case of Pb^{2+} (Figure 2). The competitive titration results suggests that the **L** is highly selective to only Fe^{3+} among all the metal ions studied, including Fe^{2+} (S07 of the Supporting Information).

Studies with Control Molecules. In order to prove the necessity of the calix[4]arene platform and the quinoline core in the receptor property of **L**, control molecules **3** and **4** devoid of these moieties were synthesized and characterized. Fluorescence and absorption titrations carried out with **3** and

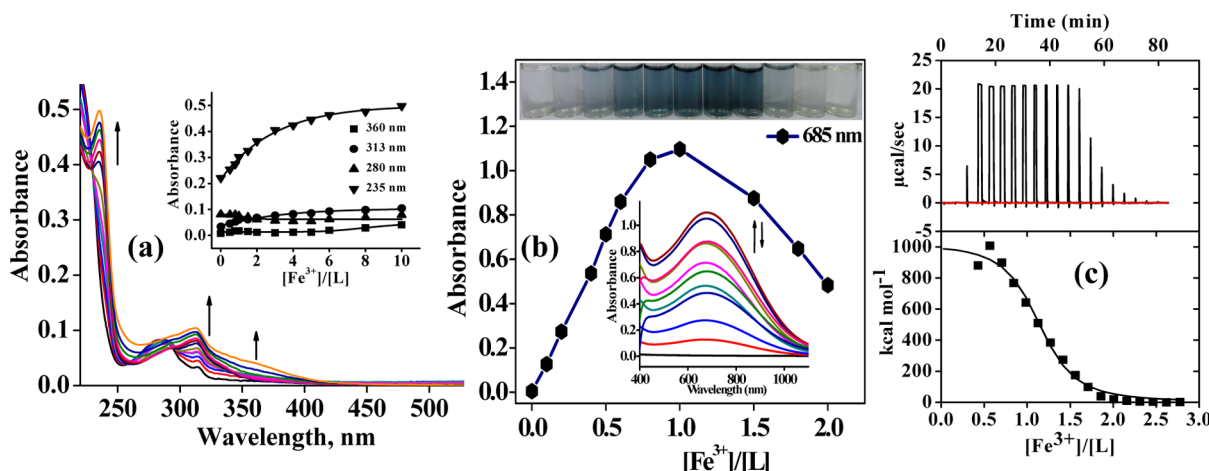


Figure 3. (a) Absorption spectra obtained during the titration of L ($5 \mu\text{M}$) with Fe^{3+} in acetonitrile. The inset shows the plot of absorbance vs $[\text{Fe}^{3+}]/[\text{L}]$ mole ratio for different absorption bands. (b) The plot of absorbance vs $[\text{Fe}^{3+}]/[\text{L}]$ mole ratio for the 685 nm band. The inset shows the absorption spectra obtained during the titration of L (0.75 mM) with Fe^{3+} in acetonitrile, and the corresponding color change observed upon the Fe^{3+} addition. (c) ITC data for L with Fe^{3+} in acetonitrile. The upper panel is baseline-corrected raw data, and the lower panel contains heats of reaction vs the mole ratio of $[\text{Fe}^{3+}]/[\text{L}]$. The solid line in the lower panel is a best fit, obtained upon using the one site model.

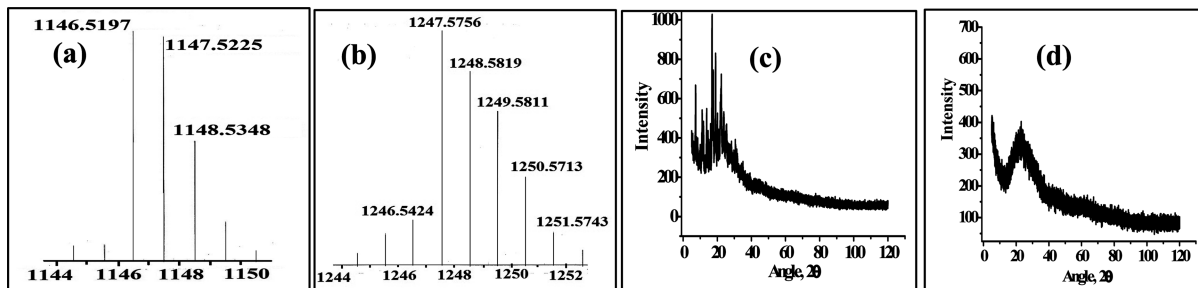


Figure 4. (a) ESI-HRMS spectrum of the $[\text{L} + \text{Fe}]^+$ complex. (b) ESI-MS spectrum of $[\text{L} + \text{Fe} + \text{ClO}_4]^+$ complex showing isotopic peak pattern. (c) Powder XRD pattern of L. (d) Powder XRD pattern of $\{\text{L}-\text{Fe}^{3+}\}$ complex.

4 showed no significant change in the emission and absorption spectra supporting, the importance of both quinoline and calix[4]arene moieties in the recognition process (S08 and S09 of the Supporting Information).

Absorption Studies. Absorption titrations were carried out in order to support the binding of Fe^{3+} to L (S10 and S11 of the Supporting Information). The free L exhibits bands at 280 and 315 nm. Upon the addition of Fe^{3+} , the absorbance at ~ 235 , 313, and 360 nm increases and that at 280 nm decreases as a function of the increase in $[\text{Fe}^{3+}]$ (Figure 3). The stoichiometry of the complex formed between L and Fe^{3+} is 1:1 as determined based on Job's plot (S12 of the Supporting Information). Absorption spectra recorded at a higher concentration of L with Fe^{3+} exhibits a band at 685 nm that is attributable to the phenolate to the Fe^{3+} charge transfer transition, and such transitions were reported in the literature.⁷ The absorbance was found to be maximum up to the addition of one equivalent of Fe^{3+} through exhibiting visually noticeable color. Addition of Fe^{3+} beyond this brings a decrease in the absorbance at 685 nm, along with the decolorization of the corresponding solutions as given in the inset of Figure 3. Thus, the data suggest that the initial one equivalent of Fe^{3+} preferably binds to the lower rim through phenolate oxygens, in addition to the triazole nitrogens. Further addition of Fe^{3+} prefers to bind to the quinoline region, which in turn brings conformational changes, resulting in the dechelation of Fe^{3+} as observed from the absorption of the 685 nm band, as well as

from the color change. An isothermal titration calorimetry study of L with Fe^{3+} (Figure 3c and S13 of the Supporting Information) shows endothermic heat change with a positive entropy, suggesting its entropic favorability. The titration yields the number of binding sites as 1, with an association constant of $K_a = (3.4 \pm 0.8) \times 10^5 \text{ M}^{-1}$, thus suggesting the formation of a 1:1 complex with moderate binding characteristics, and this value is close to that observed from the fluorescence data.

Electrospray Mass Spectrometry and Powder XRD. The stoichiometry of the complex formed between L and Fe^{3+} , both at low and high concentrations of metal ion, were established based on ESI-MS titrations. During the titration of L with Fe^{3+} , at its lower equivalents, the molecular ion peak was observed at $m/z = 1146.52 \{[\text{L}(-2\text{H}) + \text{Fe}]^+\}$ and $m/z = 574.52 \{m/2 of 1148.52 of [\text{L} + \text{Fe}]^{2+}\}$. However, at higher equivalents of Fe^{3+} , the molecular ion peak was observed at $\sim 1247.52 \{[\text{L} + \text{Fe} + \text{ClO}_4^-]^+\}$. The isotopic peak pattern observed in all these cases is characteristic for the presence of iron supporting the complex formation (Figure 4, panels a and b) of L with Fe^{3+} (S14 of the Supporting Information). While L shows marginal X-ray diffraction suggesting low crystallinity, its complex of Fe^{3+} exhibits a powder XRD that is suggestive of the noncrystalline nature (Figure 4, panels c and d), hence no structure could be determined either for L or for its Fe^{3+} complex, as none of these yielded any single crystals suitable for XRD.

NMR Titrations of L with Fe^{3+} . In order to further support the complex formation between L and Fe^{3+} , ^1H NMR titration

experiments were carried out. During the titration, the concentration of **L** was kept constant and the added $[Fe^{3+}]$ mole ratio was varied up to 2.0 equivalents. Addition of Fe^{3+} into the solution of **L** in CD_3CN , the proton NMR signals corresponding to the lower rim, viz. triazole-H (●), calix-OH (●), and the bridged $-CH_2$ group, are affected considerably, owing to the initial binding of the Fe^{3+} in the region of the lower rim (Figure 5). Further, the quinoline-H (○, ▲, Δ, ★) and

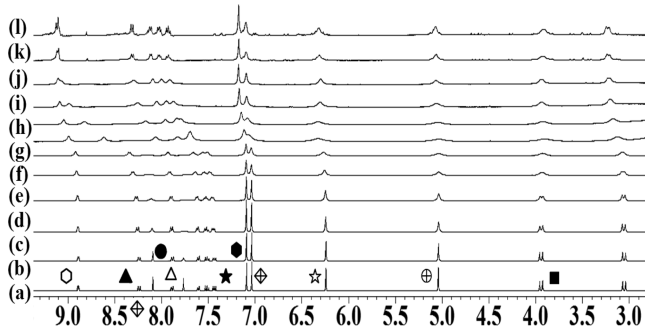


Figure 5. 1H NMR spectra measured during the titration of **L** (11.4 mM) with different mole ratio of Fe^{3+} CD_3CN ; $[Fe^{3+}]/[L]$ ratios are, (a) 0; (b) 0.05; (c) 0.075; (d) 0.10; (e) 0.125; (f) 0.25; (g) 0.50; (h) 0.75; (i) 1.0; (j) 1.25; (k) 1.75; (l) 2.0. Quinoline-H = ○, ▲, Δ, ★; triazole-H = ●; calix-OH = ●; calix-ArH = white diamond with plus sign inside; bridged CH_2 protons = ☆, ⊕, ■.

and triazole- CH_2 (☆) protons experience considerable broadening along with marginal chemical shift only at a higher mole ratio of Fe^{3+} . At a higher mole ratio (~1.5 to 2 equivalents), some of the broadened 1H NMR signals turns sharper and are resolved. On the basis of the 1H NMR titrations, it can be proposed that the Fe^{3+} initially binds to the lower rim region (calix-OH and triazole region, N_2O_4 core) and upon addition of more equivalents, the additional Fe^{3+} goes to the quinoline region that further induces the dechelation of Fe^{3+} at the lower rim region, owing to the conformation changes. Such binding is supported even by absorption studies. Variation observed in the mass spectral species seem to convey that the binding of Fe^{3+} is at two different regions of the receptor as a function of the mole ratio of the Fe^{3+} added.

Modeling the Complex of **L with Fe^{3+} Using DFT.** On the basis of all the data, it is understood that Fe^{3+} forms a 1:1 complex in the lower rim region at a low mole ratio and in the quinoline region at a high mole ratio. These complexes were modeled by DFT using **L'**, which is derived⁸ from **L** by replacing each *tert*-butyl moiety by a hydrogen. Thus, the free **L'** and both the complexes of species of recognition, viz. $[L'(Fe_a)]^+$ and $[L'(Fe_b)]^{3+}$, were studied (S15–S18 of the Supporting Information) and the corresponding optimized⁹ structures were shown in Figure 6. In the structure of $[L'(Fe_a)]^+$, the Fe_a exhibits distorted octahedral geometry with N_2O_4 coordination by bonding through two, each from phenolate oxygens, ether oxygens, and triazole nitrogens. The Fe_b in $[L'(Fe_b)]^{3+}$ exhibits a N_4 coordination by bonding through two nitrogens, each from triazole and quinoline moieties, resulting in a tetrahedral geometry.

Molecular orbitals (MOs) were calculated for **L'**, $[L'(Fe_a)]^+$, and $[L'(Fe_b)]^{3+}$ using the B3LYP/6-31G(d,p) level (Figure 7 and Figure S19 of the Supporting Information). In $[L'(Fe_a)]^+$ and $[L'(Fe_b)]^{3+}$, HOMOs were found to be majorly localized on the arene core of calix[4]arene, while these are localized on the lower rim in the case of simple **L'**. The LUMOs of $[L'(Fe_a)]^+$ are present more on the triazole as compared to the quinoline moieties, though these were extended onto the arene core moieties. In the case of $[L'(Fe_b)]^{3+}$, the LUMOs are majorly localized on triazole and quinoline. However, the LUMOs are mostly localized on quinoline only in the case of **L'**. Therefore, the computational studies further support the involvement of both the quinoline and triazole cores to bind Fe^{3+} in both complexes.

The geometry optimization of these complexes resulted in conformational changes at the arms in order to accommodate iron, which can be gauged from the dihedral angles and also the distance between the arms (S20 and S21 of the Supporting Information). During the optimization, the quinoline moieties were spread out, and the nitrogens of the triazole moieties turned to the interior of the calixarene to form an N_2O_4 core to bind to Fe_a . In the case of $[L'(Fe_b)]^{3+}$, the triazole moieties come closer to form the quinoline core to accommodate Fe_b .

Recognition under Oxidative and Reductive Conditions. In order to know the selective fluorescence enhancement as well as color changes for Fe^{3+} in comparison with Fe^{2+} , fluorescence titrations were performed with **L**, by taking the

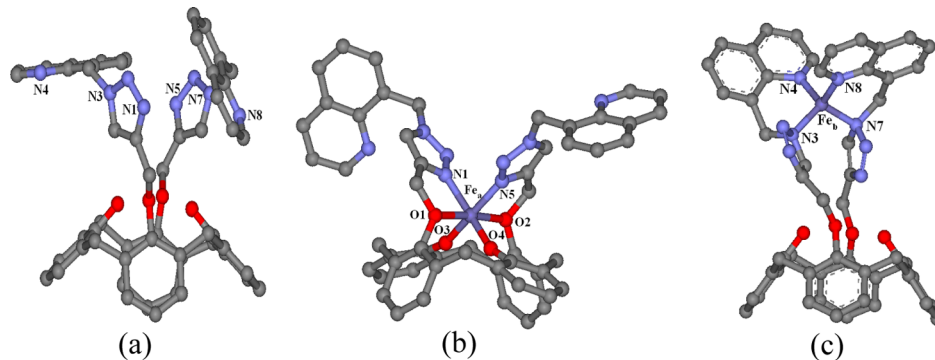


Figure 6. B3LYP/6-31G(d,p) optimized structure of (a) **L'**, (b) $[L'(Fe_a)]^+$, and (c) $[L'(Fe_b)]^{3+}$. Bond lengths (\AA) and bond angles ($^\circ$) in the primary coordination sphere of $[L'(Fe_a)]^+$: O1- Fe_a = 1.82, O2- Fe_a = 1.82, O3- Fe_a = 2.01, O4- Fe_a = 2.01, N1- Fe_a = 1.95, N5- Fe_a = 1.95; O1- Fe_a -O2 = 99.2, O1- Fe_a -O3 = 90.2, O1- Fe_a -O4 = 86.5, O1- Fe_a -N1 = 89.6, O1- Fe_a -N5 = 164.0, O2- Fe_a -O3 = 86.8, O2- Fe_a -O4 = 89.7, O2- Fe_a -N1 = 164.3, O2- Fe_a -N5 = 89.4, O3- Fe_a -O4 = 174.9, O3- Fe_a -N1 = 80.1, O3- Fe_a -N5 = 103.5, O4- Fe_a -N1 = 103.7, O4- Fe_a -N5 = 80.1, N1- Fe_a -N5 = 85.0, and in the primary coordination sphere of $[L'(Fe_b)]^{3+}$: N3- Fe_b = 1.92, N4- Fe_b = 1.89, N7- Fe_b = 1.88, N8- Fe_b = 1.84, N3- Fe_b -N4 = 105.7, N3- Fe_b -N7 = 112.4, N3- Fe_b -N8 = 111.9, N4- Fe_b -N8 = 109.9, N7- Fe_b -N8 = 102.7.

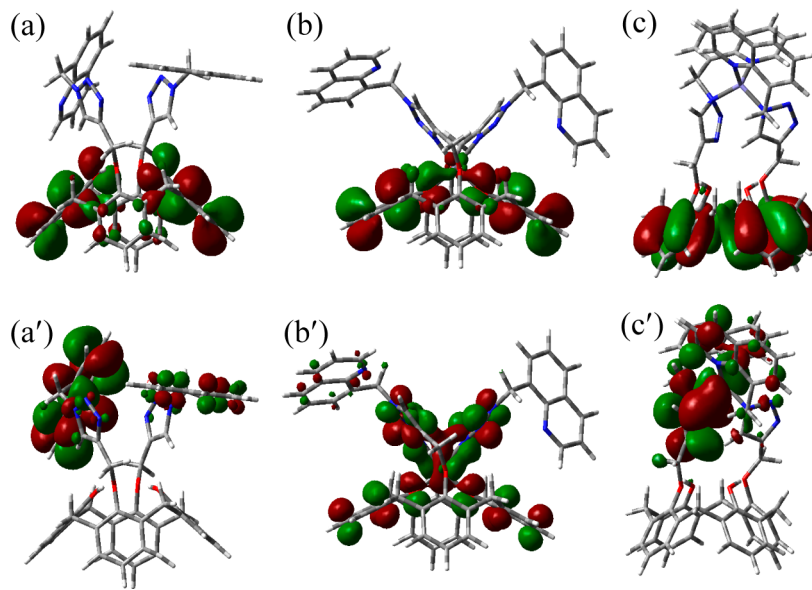


Figure 7. Pictorial representation of the molecular orbital (MOs) present on different fragments: (a), (b), and (c) are the HOMOs of L' , $[\text{L}'(\text{Fe}_\text{a})]^+$, and $[\text{L}'(\text{Fe}_\text{b})]^{3+}$, respectively. (a'), (b'), and (c') are the LUMOs corresponding to (a–c), respectively.

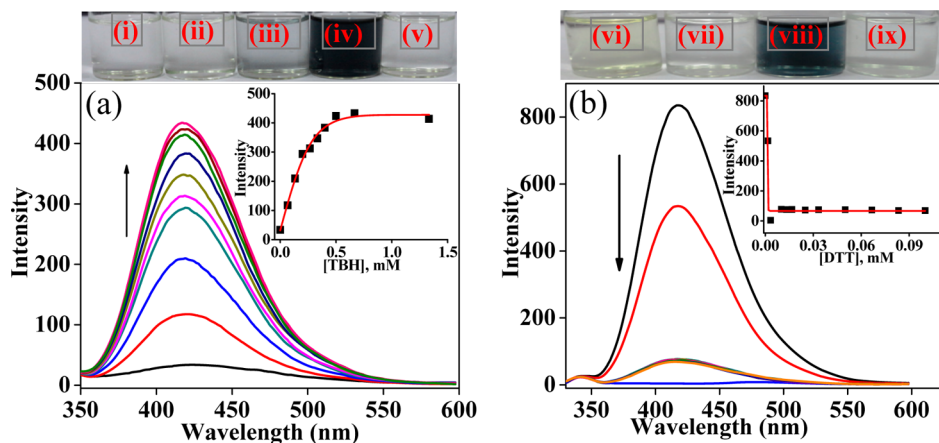


Figure 8. (a) Fluorescence spectra obtained during the titration of $[\text{L} + \text{Fe}^{2+}/\text{Fe}^{3+}]$ in the presence of an oxidizing and reducing agent, $\lambda_{\text{ex}} = 310 \text{ nm}$. (a) $[\text{L} + \text{Fe}^{2+}] + \text{TBH}$, $[\text{L}] = 10 \mu\text{M}$, and $[\text{Fe}^{2+}] = 50 \mu\text{M}$. (b) $[\text{L} + \text{Fe}^{3+}] + \text{DTT}$, $[\text{L}] = 1 \mu\text{M}$, $[\text{Fe}^{3+}] = 10 \mu\text{M}$. The inset shows the fluorescence intensity (I/I_0) as a function of the $[\text{TBH} \text{ or } \text{DTT}]/[\text{L} + \text{Fe}^{2+}/\text{Fe}^{3+}]$ mole ratio. The picture in the top row of each panel shows visual color changes observed during the oxidation and reduction events: (i) L , (ii) Fe^{2+} , (iii) $\text{L} + \text{Fe}^{2+}$, (iv) $[\text{L} + \text{Fe}^{2+}] + \text{TBH}$, (v) $\text{L} + \text{TBH}$, (vi) Fe^{3+} , (vii) $\text{Fe}^{3+} + \text{DTT}$, (viii) $\text{L} + \text{Fe}^{3+}$, and (ix) $[\text{L} + \text{Fe}^{3+}] + \text{DTT}$.

oxidizing agent {*tert*-butylhydroperoxide (TBH)} along with Fe^{2+} and the reducing agent {dithiothreitol (DTT)} along with Fe^{3+} . Fluorescence enhancement was observed upon addition of increasing amounts of TBH. The fluorescence enhancement can be attributed to the binding of in situ generated Fe^{3+} from Fe^{2+} , in the presence of TBH (S19 of the Supporting Information). This was further corroborated by the visual color change experiments carried out at higher concentration through asserting that the L to Fe^{3+} ratio is 1:1 (Figure 8). In another type of experiment, the highly fluorescent mixture containing ($\text{L} + \text{Fe}^{3+}$) was titrated with the reducing agent DTT and found successive decrease in fluorescence intensity that was further supported by an observed color change at higher mole ratios. Thus, the data suggests that the calix[4]-arene conjugate is robust enough to recognize the events of the oxidation and reduction of iron (+2 to +3 and vice versa) through exhibiting the fluorescence turn on and off. These were

further supported by color changes observable by the naked eye.

Use of $\{\text{L} + \text{Fe}^{3+}\}$ as Intracellular Fluorescent Agent.

After trypsinization, the MDA-MB-231 cells were seeded onto a 6-well plate at a density of 5000 cells per square centimeter and incubated overnight. The medium was removed, and the cells were washed with DPBS, which was followed by fixation with 4% paraformaldehyde in PBS solution for 15 to 20 min. Fixative was removed and the cells were washed twice with prewarmed PBS at 37°C . In order to establish the entry of the iron complex of L into the cells, MDA-MB-231 cells were incubated with 5 μL of a mixture of {100 μL of L (2 mM) + 100 μL of Fe^{3+} (10 mM)} for overnight at 37°C and 5% CO_2 . At this stage, the cells were visualized under a fluorescence inverted microscope (Olympus IX-81 inverted epifluorescence microscope) using a DAPI filter (excitation BP330-385 emission: BA420) and found bright intracellular blue fluorescence distributed in the cytoplasm and around the nucleus (Figure

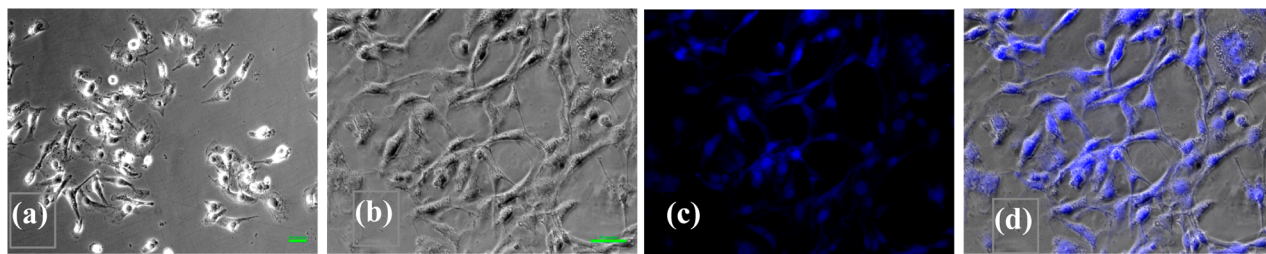


Figure 9. (a) Phase contrast microscopy picture of the control fixed MDA-MB-231 cells. (b–d) are phase contrast, fluorescent, and overlay images, respectively, of these cells upon treatment with $\{L + Fe^{3+}\}$. The scale bars of all the images are 50 μm .

9). These results were compared against the studies carried out with simple iron salt and L separately and found that there is no fluorescence signals observed under these conditions (S20 of the Supporting Information). Thus, the complex $\{L + Fe^{3+}\}$ can permeate through a biological membrane. Because of the strong fluorescence properties of $\{L + Fe^{3+}\}$, this complex can label animal cells efficiently and can work as an intracellular fluorescent agent.

Molecular Logic Gate. The conjugate, L, has been demonstrated as a molecular system that exhibits combinational logic gate properties based on three inputs of $[Fe^{3+}]$, $[Fe^{2+}]$, and TBH, and the fluorescence emission of L at 418 nm as output. In order to bring the molecular system in responding to the combinational logic gate, the output of the AND logic gate (constructed based on the inputs of Fe^{2+} and TBH) and Fe^{3+} are used to construct the OR logic gate. The inputs of $[Fe^{2+/3+}]$ and TBH were considered to be “1” when they were added and “0” when they were absent, and similarly, the output was defined as 1 in the case of fluorescence enhancement and 0 in the case of no change in fluorescence intensity (Figure 10).

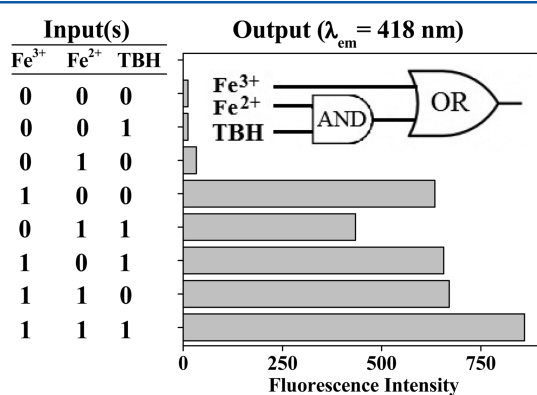


Figure 10. Histogram showing the fluorescence changes of L based on eight different inputs for the combinational logic gate.

Under the eight combinations of these inputs (Fe^{3+} , Fe^{2+} , and TBH), the first three conditions, (000), (010), and (001), exhibit no change in the fluorescence intensity of L, through exhibiting the output as “OFF” with the readout signal as 0. However, the rest of the five combinations show enhancement in the fluorescence through exhibiting the output as “ON” with the readout signal as 1.

CONCLUSIONS AND CORRELATIONS

The quinoline appended triazole linked calix[4]arene conjugate (L) has been synthesized and characterized. The conjugate exhibits a fluorescence turn on response for Fe^{3+} , among the seventeen different metal ions studied, including Fe^{2+} . All the

studies of emission, absorption, 1H NMR, and color change experiments suggested the binding of Fe^{3+} initially at the lower rim region when the mole ratio is low and later at the quinoline region when the mole ratio is high. The Fe^{3+} binding has been further confirmed by ESI-MS and ITC. The events of recognition have been simulated by computational calculations to result in a distorted octahedral N_2O_4 binding core for Fe^{3+} at low mole ratios and a tetrahedral N_4 core at higher mole ratios that is triggered by arm conformational changes. The discrimination of Fe^{3+} from that of the Fe^{2+} has been well-demonstrated by providing conditions suitable for oxidation and reduction of iron, followed by measuring the fluorescence response of L. The complex of $\{L + Fe^{3+}\}$ has been shown to enter the cytoplasm of MDA-MB-231 fixed cells by fluorescence imaging.

Further, the conjugate, L, has been utilized to demonstrate the combinational logic gate properties based on three inputs, viz. $[Fe^{2+}]$, $[Fe^{3+}]$, and TBH, and the output is the fluorescence response of L. L can detect Fe^{3+} up to 19 ± 4 ppb (338 nM) by turn on fluorescence, suggesting its applicability to detect and discriminate Fe^{3+} in the nanomolar range. Therefore, L can be used as a sensitive and selective turn on fluorescence receptor for Fe^{3+} and to successfully discriminate this from Fe^{2+} . This kind of selective and sensitive detection and discrimination of Fe^{3+} may find its use in biological assays in the real-time applications.

ASSOCIATED CONTENT

S Supporting Information

Additional information as noted in text. This material is available free of charge via the Internet at <http://pubs.acs.org>.

AUTHOR INFORMATION

Corresponding Author

*Email: cprao@iitb.ac.in. Tel: +91 22 2576 7162. Fax: +91 22 2572 3480.

Notes

The authors declare no competing financial interest.

ACKNOWLEDGMENTS

C.P.R. acknowledges the financial support from DST, CSIR, and DAE-BRNS. R.K.P. and V.K.H acknowledge CSIR for their fellowships. J.D. acknowledges DRDL, Hyderabad, for allowing him to pursue the Ph.D. program at IIT Bombay.

REFERENCES

- (a) Dunn, L. L.; Rahmanto, Y. S.; Richardson, D. R. *Trends Cell Biol.* 2007, 17, 93. (b) Weizman, H.; Ardon, O.; Meister, B.; Libman, J.; Dwir, O.; Hadar, Y.; Chen, Y.; Shanzer, A. *J. Am. Chem. Soc.* 1996, 118, 12368.

- (2) (a) Halliwell, B.; Chirico, S. *Am. J. Clin. Nutr.* **1993**, *57*, 715S.
(b) Walter, P. B.; Knutson, M. D.; Paler-Martinez, A.; Lee, S.; Xu, Y.; Viteri, F. E.; Ames, B. N. *Proc. Natl. Acad. Sci. USA* **2002**, *99*, 2264.
(c) Sen, S.; Sarkar, S.; Chattopadhyay, B.; Moirangthem, A.; Basu, A.; Dharad, K.; Chattopadhyay, P. *Analyst* **2012**, *137*, 3335. (d) Mei, Q.; Jiang, C.; Guan, G.; Zhang, K.; Liu, B.; Liua, R.; Zhang, Z. *ChemComm* **2012**, *48*, 7468. (e) Ercal, N.; Gurer-Orhan, H.; Aykin-Burns, N. *Curr. Top. Med. Chem. (Sharjah, United Arab Emirates)* **2001**, *1*, 529.
(f) Wang, J.; Pantopoulos, K. *Biochem. J.* **2011**, *434*, 365.
- (3) (a) Li, P.; Fang, L.; Zhou, H.; Zhang, W.; Wang, X.; Li, N.; Zhong, H.; Tang, B. *Chem.—Eur. J.* **2011**, *17*, 10520. (b) Li, P.; Xiao, H.; Tang, B. *Chin. J. Chem.* **2012**, *30*, 1992.
- (4) (a) Mitra, A.; Ramanujam, B.; Rao, C. P. *Tetrahedron Lett.* **2009**, *50*, 776. (b) Wolf, C.; Mei, X.; Rokadia, H. K. *Tetrahedron Lett.* **2004**, *45*, 7867. (c) Lohani, C. R.; Lee, K.-H. *Sens. Acutators, B* **2010**, *143*, 649. (d) Singh, N.; Kaur, N.; Dunn, J.; Mackay, M.; Callan, J. F. *Tetrahedron Lett.* **2009**, *50*, 953. (e) Lee, D. Y.; Singh, N.; Jang, D. O. *Tetrahedron Lett.* **2011**, *52*, 1368. (f) Lin, W.; Long, L.; Yuan, L.; Cao, Z.; Feng, J. *Anal. Chim. Acta* **2009**, *634*, 262. (g) Zhang, M.; Gao, Y.; Li, M.; Yu, M.; Li, F.; Li, L.; Zhu, M.; Zhang, J.; Yi, T.; Huang, C. *Tetrahedron Lett.* **2007**, *48*, 3709. (h) Wang, S.; Meng, X.; Zhu, M. *Tetrahedron Lett.* **2011**, *52*, 2840. (i) Kumar, M.; Kumar, R.; Bhalla, V.; Sharma, P. R.; Kaur, T.; Qurishi, Y. *Dalton Trans.* **2012**, *41*, 408.
(j) Zhan, J.; Wen, L.; Miao, F.; Tian, D.; Zhu, X.; Li, H. *New J. Chem.* **2012**, *36*, 656. (k) Sahoo, S. K.; Sharma, D.; Bera, R. K.; Crisponi, G.; Callan, J. F. *Chem. Soc. Rev.* **2012**, *41*, 7195. (l) Liu, J.-M.; Zheng, Q.-Y.; Yang, J.-L.; Chen, C.-F.; Huang, Z.-T. *Tetrahedron Lett.* **2002**, *43*, 9209. (m) Ocak, U.; Ocak, M.; Surowiec, K.; Liu, X. D.; Bartsch, R. A. *Tetrahedron* **2009**, *65*, 7038.
- (5) (a) Chen, X.; Pradhan, T.; Wang, F.; Kim, J. S.; Yoon, J. *Chem. Rev.* **2012**, *112*, 1910. (b) Kim, H. N.; Lee, M. H.; Kim, H. J.; Kim, J. S.; Yoon, J. *Chem. Soc. Rev.* **2008**, *37*, 1465. (c) Aydin, Z.; Wei, Y.; Guo, M. *Inorg. Chem. Commun.* **2012**, *20*, 93.
- (6) (a) Benesi, H. A.; Hildebrand, J. H. *J. Am. Chem. Soc.* **1949**, *71*, 2703. (b) Mukhopadhyay, M.; Banerjee, D.; Koll, A.; Mandal, A.; Filarowski, A.; Fitzmaurice, D.; Das, R.; Mukherjee, S. *J. Photochem. Photobiol., A* **2005**, *125*, 94.
- (7) Carrano, C. J.; Carrano, M. W.; Sharma, K.; Backes, G.; Sanders-Loehr, J. *Inorg. Chem.* **1990**, *29*, 1865.
- (8) Pathak, R. K.; Hinge, V. K.; Mondal, P.; Rao, C. P. *Dalton Trans.* **2012**, *41*, 10652.
- (9) Frisch, M. J.; et al. *Gaussian 03*, revision C.02; Gaussian, Inc.: Wallingford, CT, 2004 (all the authors of this publication are listed in S21 of the Supporting Information).